Journal of Electrical and Electronic Engineering
2022; 10(4): 162-169
http://www.sciencepublishinggroup.com/j/jeee
doi: 10.11648/j.jeee.20221004.15
ISSN: 2329-1613 (Print); ISSN: 2329-1605 (Online)

Fiber Fuse Simulation in Multi-Core Fibers for Space Division Multiplexed Transmission

Yoshito Shuto

Ofra Project, Iruma, Japan

Email address:
ofra@tuba.ocn.ne.jp

To cite this article:
Yoshito Shuto. Fiber Fuse Simulation in Multi-Core Fibers for Space Division Multiplexed Transmission. *Journal of Electrical and Electronic Engineering.* Vol. 10, No. 4, 2022, pp. 162-169. doi: 10.11648/j.jeee.20221004.15

Received: August 7, 2022; **Accepted**: August 23, 2022; **Published**: August 31, 2022

Abstract: Owing to the progress of dense wavelength-division multiplexing (WDM) technology using an optical-fiber amplifier, we can exchange large amounts of data at a rate of 100 Tbit/s class over several hundred kilometers. However, it is widely recognized that the maximum transmission capacity of a single strand of fiber is rapidly approaching its limit of ~100 Tbit/s owing to the optical power limitations imposed by the fiber fuse phenomenon and the finite transmission bandwidth determined by optical-fiber amplifiers. To overcome these limitations, space-division multiplexing (SDM) technologies using a multi-core fiber (MCF) were proposed. The fiber fuse experiments of MCFs at 1.55 μm were conducted using two types of MCFs: homogeneous 7-core MCF and heterogeneous 6-core MCF. The fiber fuse effect in these MCFs was studied theoretically by the explicit finite-difference method using the thermochemical SiO_x production model. In the calculation, we assumed that two types of MCFs have a simple refractive-index profile, which is similar to that of doubly clad single-mode fibers. The calculated threshold power P_{th} of the homogeneous MCF was 1.19-1.25 W, which was close to the experimental P_{th} value of SMF. On the other hand, the P_{th} of small core fiber in heterogeneous MCF was 0.89 W. It was found that the P_{th} values of two types of MCFs were proportional to their cross sectional area A_{eff} values. Next, the cross sectional area A of the vaporized core was estimated using the proportionality constant V_f / P_0 of MCFs and SMF at $P_0 \geq 5$ W. The A values of homogeneous MCF and SMF were close to their A_{eff} values. On the other hand, the A value of small core fiber in heterogeneous MCF was larger than its A_{eff} value. From these results, it was concluded that the plasma, which occurred in the vaporized core, tends to expand in the small-A_{eff} fiber. Furthermore, it was found that in the neighboring core layers the generation and propagation of fiber fuse was hindered during fiber fuse propagation in the heated core of homogeneous and/or heterogeneous MCF.

Keywords: Fiber Fuse Phenomenon, Multi-Core Fibers, Finite-Difference Technique

1. Introduction

Silica-based optical fibers are the most important transmission medium for long-distance and large-capacity optical communication systems. Owing to the progress of dense wavelength-division multiplexing (WDM) technology using an optical-fiber amplifier, we can exchange large amounts of data at a rate of 100 Tbit/s class over several hundred kilometers [1].

However, it is widely recognized that the maximum transmission capacity of a single strand of fiber is rapidly approaching its limit of ~100 Tbit/s owing to the optical power limitations imposed by the fiber fuse phenomenon and the finite transmission bandwidth determined by optical-fiber amplifiers [2-4].

To overcome these limitations, space-division multiplexing (SDM) technologies using a multi-core fiber (MCF), few-mode fiber (FMF), and few-mode multi-core fiber (FM-MCF) were proposed [2-9], and Pbit/s class transmission was demonstrated using these multi-core fibers [10-19].

In a conventional (uncoupled) MCF, several cores exist in an optical fiber, as shown in Figure 1.

In this figure, seven cores arranged in a hexagonal array, and Λ and h_c are the distance (pitch) between the core centers and the outer cladding thickness, respectively. If all the cores are identical to each other, the core density is mainly dominated by Λ, which guarantees a required crosstalk level along a given propagation length.

Takenaga *et al*. investigated several seven-core MCF, as shown in Figure 1, and found that all the MCFs with Λ =

40-43 μm exhibit crosstalk of less than -30dB at a propagation length of 100 km and a wavelength (λ_0) of 1.55 μm [20]. They also found that the reduction of h_c will be limited by the occurrence of the excess loss on outer cores and the h_c should be larger than 38 μm to suppress the excess losses of the outer cores less than 0.001 dB/km [20].

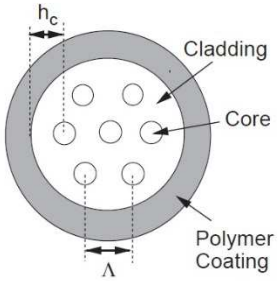

Figure 1. *Schematic of seven-core MCF.*

On the other hand, it is well known that when the refractive indices or radii of the cores are slightly different from each other, the maximum power transferred between the cores decreases drastically [21, 22]. Using this benefit, a heterogeneous MCF was proposed by Koshiba and coworkers [23]. In the heterogeneous MCFs, not only identical but also non-identical cores are arranged in a optical fiber so that crosstalk between any pair of cores becomes sufficiently small [23]. As a result, cores of the heterogeneous MCFs are more closely packed in definite space, compared to a conventional, homogeneous MCF composed of only identical cores.

Homogeneous and heterogeneous MCFs with a large effective cross sectional area (A_{eff}) of > 70 μm^2 at λ_0 = 1.55 μm are realized by several research institutes [6, 20, 24-29]. These MCFs are effective for preventing the occurrence of fiber fuse effect by lowering the optical power density of the core in each waveguide.

The fiber fuse experiments of MCFs at λ_0 = 1.55 μm were reported in 2012 by Sekiya *et al*. [30]. In this article, we investigated the unsteady-state thermal conduction process in MCFs theoretically with the explicit finite-difference method using the thermochemical SiO_x production model [31].

2. Fiber Fuse Effect of MCFs

The fiber fuse experiments of multi-core fibers were conducted for the first time by Sekiya and co-workers [30].

Fiber fuse was generated with exposure to arc discharge provided by a fusion splicer [32].

They investigated two types of MCFs shown in Figure 2. The MCF type 1 (MCF1) consists of 7 identical single-mode (SM) cores, which is numbered from 0 to 6, as shown in Figure 2(a).

In contrast, the MCF type 2 (MCF2) consists of 3 identical SM cores being numbered from 1 to 3, intercalated with 3 identical small cores A, B, and C, whose diameters are smaller than those of SM cores, as shown in Figure 2(b).

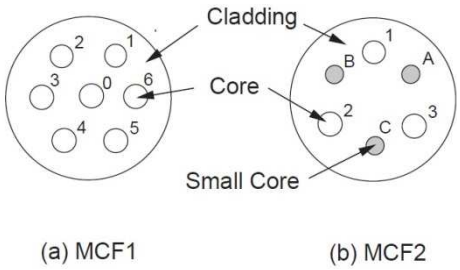

Figure 2. *Two types of MCFs.*

2.1. Parameters of MCFs

The parameters and refractive-index profiles of the MCF1 and MCF2 are not described in the literature [30]. In the calculation, we set the core pitch Λ to 40 μm and the outer cladding thickness h_c to 45 m.

It is well known that a trench-assisted MCF design is widely used in the conventional and heterogeneous MCFs [20, 24, 25, 28]. The refractive-index profile of the trench-assisted MCF is shown in Figure 3(a).

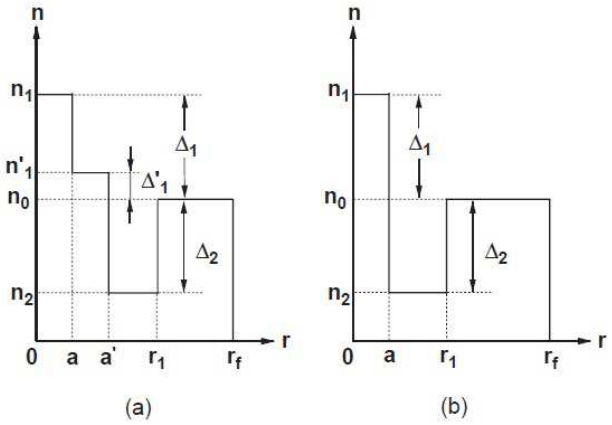

Figure 3. *Refractive-index profile of MCF.*

In this figure, a, a', and r_1 are the radii of the (first) core, second core, and trench, respectively, and n_1, n'_1, n_0, and n_2 are the refractive indices in the (first) core, second core, cladding, and trench, respectively. r_f is the cladding radius. As shown in Figure 3(a), a trench-assisted MCF has a dual-shape or convex-index profile of the core [33-35] and its refractive-index profile is somewhat complicated.

Therefore, in the calculation, we assumed that MCF1 and/or MCF2 have a simple refractive-index profile as shown in Figure 3(b). These MCFs are regarded as doubly clad single-mode fibers [36-39].

The relative refractive-index difference Δ_1 and Δ_2 in Figure 3 are defined as

$$\Delta_1 = \frac{(n_1^2 - n_0^2)}{2n_1^2} \sim \frac{(n_1 - n_0)}{n_1} \quad (1)$$

$$\Delta_2 = \frac{(n_2^2 - n_0^2)}{2n_2^2} \sim \frac{(n_2 - n_0)}{n_2} \quad (2)$$

The parameters of two MCFs are shown in Table 1, together with a conventional step-index SMF.

Table 1. *Parameters of MCFs and step-index SMF.*

Parameters	MCF 1-0	MCF 1-1-6	MCF 2-1-3	MCF 2-A-C	SMF
Δ_1 (%)	0.45	0.45	0.45	0.50	0.36
Δ_2 (%)	-0.55	-0.55	-0.55	-0.55	-
a (μm)	4	4	4	2	4.6
r_1 (μm)	5	5	5	3	-
r_f (μm)	62.5	45	45	45	62.5
A_{eff} (μm^2)	79.53	79.53	79.53	52.71	93.11

In this table, A_{eff} is the effective cross sectional area at 1.55 μm, which is defined as follows [40, 41]:

$$A_{eff} = \frac{\left[\int_0^{2\pi}\int_0^{\infty}|R(r,\theta)|^2 r dr d\vartheta\right]^2}{\int_0^{2\pi}\int_0^{\infty}|R(r,\theta)|^4 r dr d\theta} \quad (3)$$

where R (r, θ) is the electric field distribution of the fundamental LP_{01} mode of the fiber, which is expressed in cylindrical coordinates. The A_{eff} value at 1.55 μm was estimated with the finite element method (FEM) [42].

2.2. Chromatic Dispersion of MCFs

Chromatic dispersion in the 1.0-1.7-μm spectral region for the step-index SMF and the MCFs were calculated by using the FEM program. The calculated results are shown in Figure 4. It is clear that zero chromatic dispersion of MCF1-0-6 and MCF2-1-3 occurs at 1.3 μm, which is close to the zero-dispersion wavelength λ_{cd}^0 (= 1.31 μm) of the SMF.

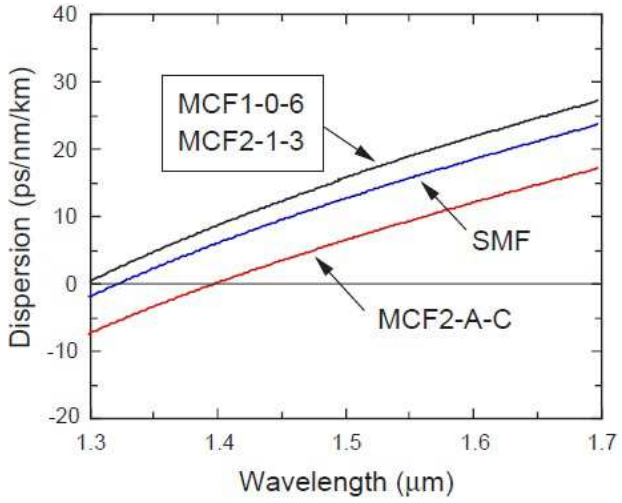

Figure 4. *Chromatic dispersion of SMF and MCFs.*

On the other hand, the zero chromatic dispersion of the MCF2-A-C occurs at 1.4 μm, which is longer than the λ_{cd}^0 of the SMF.

In the next section, we describe the results of some numerical calculations related to the thermal conduction process in MCFs described above.

3. Fiber Fuse Calculation in MCFs

We assume that the MCF is in an atmosphere of $T = T_a$. We also assume that part of the core layer is heated and has a length of ΔL (= 40 μm) and a temperature of T_c^0 (> T_a) (see Figure 5).

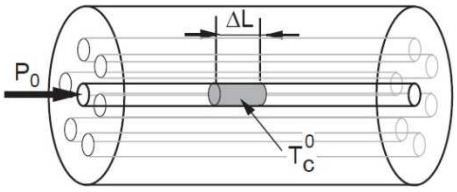

Figure 5. *Schematic view of hot zone in core layer of MCF.*

In the heating zone (called the ``hot zone") shown in Figure 5, an absorption coefficient α is larger than that in the other parts of the core because of its high temperature T_c^0 (> T_a). Thus, as the light propagates along the positive direction (away from the light source) in this zone, a considerable amount of heat is produced by light absorption.

3.1. Threshold Power in MCFs

We investigated the core center temperature distribution in the longitudinal direction of the MCF1-0 and MCF1-1 after the incidence of a laser power P_0 of up to 2 W. In the calculation, we set the time interval δt to 10 ns, the step size along the r axis δr to r_f/14 for MCF1-0 and r_f/10 for MCF1-1, and the step size along the z axis δz to 20 μm, and assumed that T_c^0 = 2,923 K and T_a = 298 K.

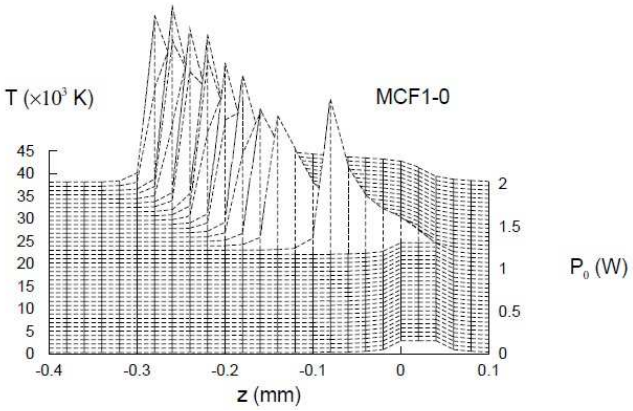

Figure 6. *Core center temperature distribution in the longitudinal direction of the MCF1-0 after 1 ms when P_0 = 0-2 W and λ_0 = 1.55 μm.*

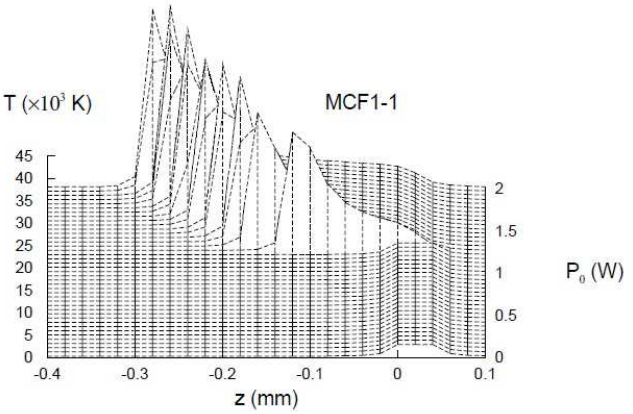

Figure 7. *Core center temperature distribution in the longitudinal direction of the MCF1-1 after 1 ms when P_0 = 0-2 W and λ_0 = 1.55 μm.*

We estimated the change in the temperature T (0, z) at the

core center (r = 0 μm) in the MCF1-0 and MCF1-1 at t = 1 ms after the incidence of laser light with λ_0 = 1.55 μm and initial power P_0 = 0-2 W. The calculated changes in the temperature at the core center position are shown in Figures 6 and 7.

When the power of the light entering the MCF1-0 increases from 1.15 W to 1.20 W, the peak temperature rises from 2,923 to 33,800 K, and thereafter, propagation behavior was observed in the -z direction with increasing P_0, as shown in Figure 6. The characteristic P_0 value of 1.20 W (or more accurately 1.19 W) is the threshold power P_{th} of the MCF1-0. This value is close to the experimental P_{th} value (1.39 W [43]) of SMF. The P_{th} of the MCF1-1 is determined as 1.25 W in the same manner as the MCF1-0, as shown in Figure 7. This value is almost same as that (1.19 W) of the MCF1-0.

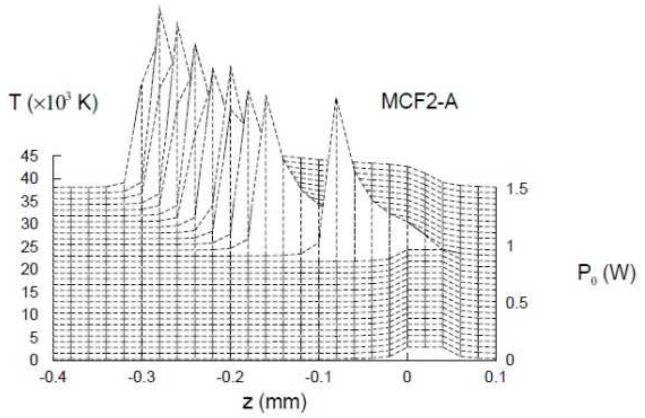

Figure 8. *Core center temperature distribution in the longitudinal direction of the MCF2-A after 1 ms when P_0 = 0-1.5 W and λ_0 = 1.55 μm.*

Furthermore, we investigated the change in the temperature T (0, z) at the core center (r = 0 μm) in the MCF2-A at t = 1 ms after the incidence of a laser power P_0 of up to 1.5 W. In the calculation, we set the step size along the r axis δr to r_f/10.

The calculated change in the temperature at the core center position is shown in Figure 8. As shown in Figure 8, when the power of the light entering the MCF2-A increases from 0.85 W to 0.90 W, the peak temperature rises from 2,923 to 35,100 K, and thereafter propagation behavior was observed in the -z direction with increasing P_0.

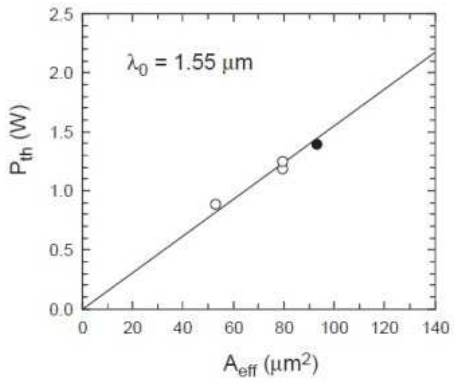

Figure 9. *Effective cross-sectional area dependence of the threshold powers at λ_0 = 1.55 μm. The closed circle is the data reported by Abedin and Nakazawa [43].*

The P_{th} of the MCF2-A is determined to 0.90 W (or more accurately 0.89 W). This value is smaller than that of the MCF1-0 (1.19 W) or MCF1-1 (1.25 W).

We examined the A_{eff} dependence of the P_{th} values at λ_0 = 1.55 μm. The results are shown in Figure 9. As shown in Figure 9, the P_{th} values are proportional to the A_{eff} values.

Similar proportional relationship between P_{th} and A_{eff} was reported in the dispersion-shifted fibers [43].

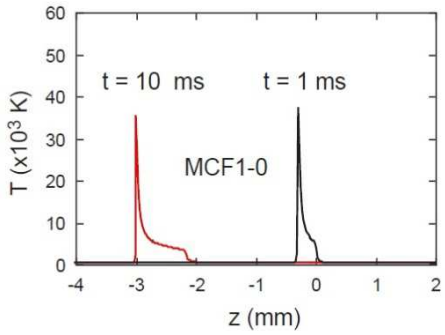

Figure 10. *Temperature fields of the core center of MCF1-0 after 1 and 10 ms when P_0 = 2 W and λ_0 = 1.55 μm.*

3.2. Relationship Between P_0 and V_f in MCFs

Next, we estimated the temperature field of the core center of the MCF1-0 along the z direction at t = 1 ms and 10 ms after the incidence of laser light with P_0 = 2 W and λ_0 = 1.55 μm. The calculated results are shown in Figure 10.

As shown in Figure 10, the core center temperature near the end of the hot zone (z = -0.28 mm) changes abruptly to a high value of about 3.7 × 10^4 K after 1 ms. This rapid rise in the temperature initiates the fiber fuse propagation. After 10 ms, the high-temperature front in the core layer reaches a z value of -2.98 mm. The average propagation velocity V_f is estimated to be 0.30 m/s using these data. This V_f is close to the value (~0.32 m/s) of SMF measured by Abedin and Nakazawa [43].

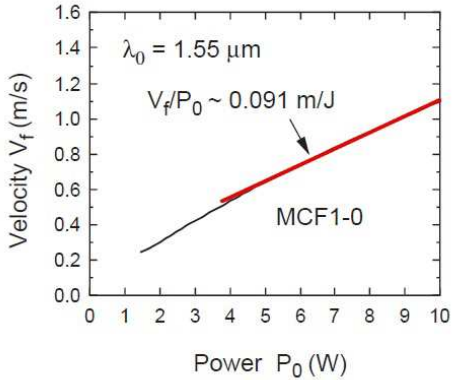

Figure 11. *Relationships between the velocity V_f and the input power P_0 for MCF1-0 at λ_0 = 1.55 μm.*

Figure 11 shows the P_0 dependence of the V_f values for MCF1-0 at λ_0 = 1.55 μm.

As shown in Figure 11, the slope V_f / P_0 of MCF1-0 decreases gradually with increasing P_0 at P_0 < 5 W and then increases linearly with increasing P_0 at P_0 ≥ 5 W. Such a

proportional relationship between V_f and P_0 was observed by Sekiya *et al*. [30]. The proportionality constant V_f / P_0 of MCF1-0 at $P_0 \geq 5$ W was estimated to be about 0.091 m/J (see Figure 11).

Figure 12 shows the P_0 dependence of the V_f values for the SMF at λ_0 = 1.55 μm. The data reported by Abedin and Nakazawa [43] are plotted in this figure.

As shown in Figure 12, the V_f values are close to the experimental values. Furthermore, the slope V_f / P_0 of SMF decreases gradually with increasing P_0 at $P_0 < 5$ W and then increases linearly with increasing P_0 at $P_0 \geq 5$ W. Similar behavior in a commercial single-mode optical fiber (SMF-28) at λ_0 = 1.48 μm was observed by Todoroki [45].

The proportionality constant V_f / P_0 of SMF at $P_0 \geq 5$ W was estimated to be about 0.081 m/J (see Figure 12).

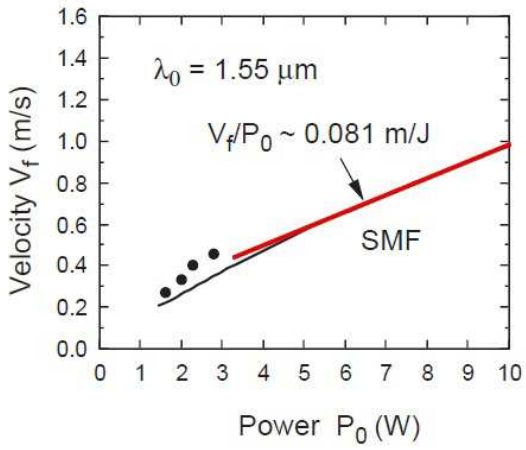

Figure 12. *Relationships between the velocity V_f and the input power P_0 for SMF at λ_0 = 1.55 μm. The closed circles are the data reported by Abedin and Nakazawa [36].*

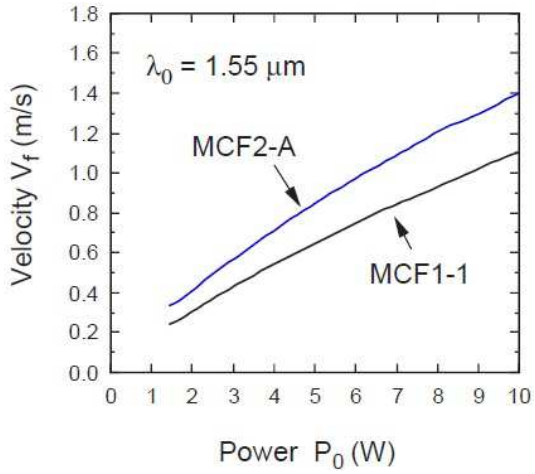

Figure 13. *Relationships between the velocity V_f and the input power P_0 for MCF1-1 and MCF2-A at λ_0 = 1.55 μm.*

Next, the P_0 dependence of the V_f values for MCF1-1 and/or MCF2-A was investigated at λ_0 = 1.55 μm. The calculated results are shown in Figure 13.

As shown in Figure 13, the slope V_f / P_0 of MCF2-A is larger than that of MCF1-1. The proportionality constant V_f / P_0 of MCF2-A at $P_0 \geq 5$ W is about 0.111 m/J, which is about 1.2 times that (0.092 m/J) of MCF1-1.

A fiber fuse is a thermal wave composed of plasma. The input power P_0 absorbed in the hot zone in the core layer is converted into heat. Although most of the heat is dissipated to the neighboring core and cladding layers, part of the heat can be used to form and propagate the thermal wave (plasma).

The reduction factor of P_0 due to internal energy loss (heat dissipation) from the fiber core is defined as f. Using f, the propagation velocity V_f of fiber fuse is given by the following equation:

$$V_f = \frac{P_0 f}{A \rho C_p \Delta T} \tag{4}$$

where ΔT is the temperature increase that results in vaporization. A, ρ (= 2,024.0 kg m^{-3}), and C_p (= 844.4 J kg^{-1} K^{-1}) are the cross-sectional area, density, and specific heat of the vaporized core, respectively.

This equation is somewhat similar in form to the models proposed by Kashyap and Blow [46] and Atkins *et al*. [47], which were assumed no energy loss from the fiber core.

We assumed that ΔT = 5,760 K, which was the average temperature of the radiation zone [31], and f = 0.07. We can estimate A by using Eq. (4) and V_f / P_0 value.

The parameters, V_f / P_0, and A values of various MCFs and SMF are shown in Table 2.

Table 2. *Parameters, V_f / P_0, and A values of various MCFs and SMF.*

Fibers	A_{eff} (μm^2)	V_f / P_0 (m/J)	A (μm^2)
MCF1-0	79.53	0.091	78.14
MCF1-1	79.53	0.092	77.29
MCF2-A	52.71	0.111	64.06
SMF	93.11	0.081	87.79

As shown in this table, the A values of MCF1-0, MCF1-1, and SMF are close to their A_{eff} values. On the other hand, the A value (64.06 μm^2) of MCF2-A is about 1.2 times the value of its A_{eff} value (52.71 μm^2).

From these results, it was concluded that the plasma, which occurred in the vaporized core, tends to expand in the small-A_{eff} fiber, such as MCF2-A.

The radius r_p of the expanded plasma in MCF2-A is about 4.52 μm. This is about 2.3 times the value (2 μm) of a, but the increment (2.52 μm) of the radius is very small, compared with the core pitch Λ of 40 μm.

3.3. Possibility of Fiber Fuse Initiation in Neighboring Cores

When fiber fuse propagation occurs in the core of MCF1-0, the heat generated in the core is transferred to the cladding layer near its periphery and the cores of its neighbors. If parts of the neighboring core layers are heated to a high temperature of $\geq T_c^0$ (= 2,923 K), a fiber fuse will be initiated in these parts of the neighboring core layers.

To elucidate this problem, the temperature fields in MCF1-0 in the course of fiber fuse propagation were calculated after 5 ms when P_0 = 10 W and λ_0 = 1.55 μm. The calculated results are shown in Figure 14.

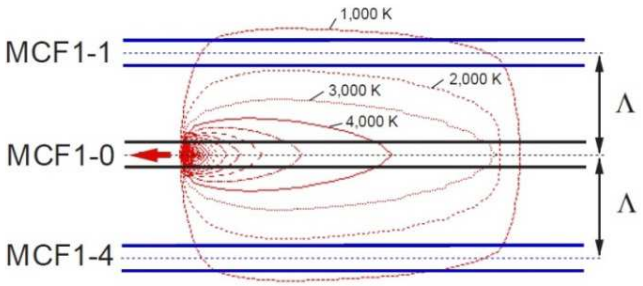

Figure 14. *Temperature distribution around the core of MCF1-0 after 5 ms when P_0 = 10 W and λ_0 = 1.55 μm.*

In this figure, the temperature distribution around the core of MCF1-0 is shown by red contour lines.

As shown in Figure 14, the maximum temperature in the neighboring core layers of MCF1-1 and MCF1-4 is lower than 2,000 K (or more accurately 1,600 K). As this temperature (< 1,600 K) is lower than T_c^0 (= 2,923 K), the generation and propagation of fiber fuse will not occur in the neighboring core layers during fiber fuse propagation in the heated core of MCF1-0.

Furthermore, the temperature fields in MCF2-A in the course of fiber fuse propagation were calculated after 5 ms when P_0 = 10 W and λ_0 = 1.55 μm. The calculated results are shown in Figure 15. In this figure, the temperature distribution around the core of MCF2-A is shown by red contour lines.

As shown in Figure 15, the maximum temperature in the neighboring core layer of MCF2-3 is lower than 2,000 K (or more accurately 1,000 K).

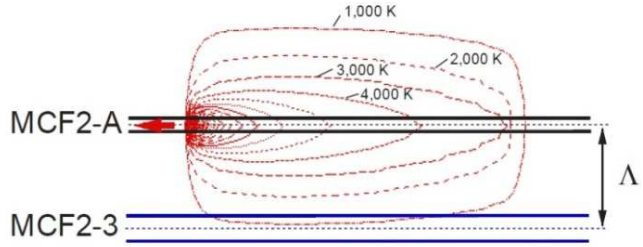

Figure 15. *Temperature distribution around the core of MCF2-A after 5 ms when P_0 = 10 W and λ_0 = 1.55 μm.*

As this temperature (< 1,000 K) is lower than T_c^0, the generation and propagation of fiber fuse will not occur in the neighboring core layers during fiber fuse propagation in the heated core of MCF2-A.

From these results, it is concluded that in the neighboring core layers the generation and propagation of fiber fuse is hindered during fiber fuse propagation in the heated core of homogeneous and/or heterogeneous MCF when P_0 of up to 10 W.

4. Conclusion

The fiber fuse experiments of MCFs at 1.55 μm were conducted using two types of MCFs: homogeneous 7-core MCF and heterogeneous 6-core MCF. The fiber fuse effect in these MCFs was studied theoretically by the explicit finite-difference method using the thermochemical SiO_x production model. In the calculation, we assumed that two types of MCFs have a simple refractive-index profile, which is similar to that of doubly clad single-mode fibers. The calculated threshold power P_{th} of the homogeneous MCF was 1.19-1.25 W, which was close to the experimental P_{th} value of SMF. On the other hand, the P_{th} of small core fiber in heterogeneous MCF was 0.89 W. It was found that the P_{th} values of two types of MCFs were proportional to their cross sectional area A_{eff} values. Next, the cross-sectional area A of the vaporized core was estimated using the proportionality constant V_f / P_0 of MCFs and SMF at $P_0 \geq 5$ W. The A values of homogeneous MCF and SMF were close to their A_{eff} values. On the other hand, the A value of small core fiber in heterogeneous MCF was larger than its A_{eff} value. From these results, it was concluded that the plasma, which occurred in the vaporized core, tends to expand in the small-A_{eff} fiber. Furthermore, it was found that in the neighboring core layers the generation and propagation of fiber fuse was hindered during fiber fuse propagation in the heated core of homogeneous and/or heterogeneous MCF.

Acknowledgements

The author is especially indebted to Dr. Katsunari Okamoto (Okamoto Laboratory) for his support with the FEM calculation program for optical fibers.

References

[1] Sano A., Kobayashi T., Yoshida E., and Miyamoto Y. (2011). Ultra-high capacity optical transmission technologies for 100 Tbit/s optical transport networks. IEICE Trans. Commun., E94-B (2), 400-408.

[2] Morioka T. (2009). New generation optical infrastructure technologies: ``EXAT initiative" toward 2020 and beyond. OptoElectron. Commun. Conf. (OECC 2009), FT4.

[3] Nakazawa M. (2014). Evolution of EDFA from single-core to multi-core and related recent progress in optical communication. Opt. Rev., 21 (6), 862-874.

[4] Morioka T., Awaji Y., Matsushima Y., and Kamiya T. (2017). R&D of 3M technologies toward the realization of Exabit/s optical communications. IEICE Trans. Commun., E100-B (9), 1707-1715.

[5] Richardson D. J., Fini J. M., and Nelson L. E. (2013). Space-division multiplexing in optical fibres. Nature Photon., 7, 354-362.

[6] Matsuo S., Takenaga K., Sasaki Y., Amma Y., Saitoh S., Matsui T., Nakajima K., Mizuno T., Takara H., Miyamoto Y., and Morioka T. (2016). High-space-multiplicity multicore fibers for future dense space-division multiplexing systems. IEEE J. Lightwave Technol., 34 (6), 1464-1475.

[7] Mizuno T., Takara H., Sano A., and Miyamoto Y. (2016). Dense space-division multiplexed transmission systems using multi-core and multi-mode fiber. IEEE J. Lightwave Technol., 34 (2), 582-592.

[8] Mizuno T. and Miyamoto Y. (2017). High-capacity dense space division multiplexing transmission. Opt. Fiber Technol., 35, 108-117.

[9] Puttnam B. J., Rademacher G., and Luis R. S. (2021). Space-division multiplexing for optical fiber communications. Optica, 8 (9), 1186-1203.

[10] Takara H., Asano A., Kobayashi T., Kubota H., Kawakami H., Matsuura A., Miyamoto Y., Abe Y., Ono H., Shikama K., Goto Y., Tsujikawa K., Sasaki Y., Ishida I., Takenaga K., Matsuo S., Saitoh K., Koshiba M., and Morioka T. (2012). 1.01-Pb/s (12 SDM/222 WDM/456 Gb/s) crosstalk-managed transmission with 91.4-b/s/Hz aggregate spectral efficiency. Eur. Conf. Opt. Commun. (ECOC2012), Th. 3. C. 1.

[11] Igarashi K., Tsuritani T., Morita I., Tsuchida Y., Maeda K., Tadakuma M., Saito T., Watanabe K., Imamura K., Sugizaki R., and Suzuki M. (2013). 1.03-exabit/s·km super-Nyquist-WDM transmission over 7,326-km seven-core fiber. Eur. Conf. Opt. Commun. (ECOC2013), PD. 3. E. 3.

[12] Puttnam B. J., Luis R. S., Klaus W., Sakaguchi J., Delgado Mendinueta J. M., Awaji Y., Wada N., Tamura Y., Hayashi T., Hirano M., and Marciante J. (2015). 2.15 Pb/s transmission using a 22 core homogeneous single-mode multi-core fiber and wideband optical comb. Eur. Conf. Opt. Commun. (ECOC2015), PDP. 3. 1.

[13] Soma D., Igarashi K., Wakayama Y., Takeshima K., Kawaguchi Y., Yoshikane N., Tsuritani T., Morita I., and Suzuki M. (2015). 2.05 peta-bit/s super-Nyquist-WDM SDM transmission using 9.8-km 6-mode 19-core fibre in full C band. Eur. Conf. Opt. Commun. (ECOC2015), PDP. 3. 2.

[14] Kobayashi T., Nakamura M., Hamaoka F., Shibahara K., Mizuno T., Sano A., Kawakami H., Isoda A., Nagatani M., Yamazaki H., Miyamoto Y., Amma Y., Sasaki Y., Takenaga K., Aikawa K., Saitoh K., Jung Y., Richardson D. J., Pulverer K., Bohn M., Nooruzzaman M., and Morioka T. (2017). 1-Pb/s (32 SDM/46 WDM/768 Gb/s) C-band dense SDM transmission over 205.6-km of single-mode heterogeneous multi-core fiber using 96-Gbaud PDM-16QAM channels. Opt. Fiber Commun. (OFC2017), Th5B. 1.

[15] Soma D., Wakayama Y., Beppu S., Sumita S., Tsuritani T., Hayashi T., Nagashima T., Suzuki M., Takahashi H., Igarashi K., Morita I., and Suzuki M. (2017). 10.16 peta-bit/s dense SDM/WDM transmission over low-DMD 6-mode 19-core fibre across C+L band. Eur. Conf. Opt. Commun. (ECOC2017), Th. PDP. A. 1.

[16] Luis R. S., Rademacher G., Puttnam B. J., Furukawa H., Ross-Adams A., Gross S., Withford M., Riesen N., Sasaki Y., Saitoh K., Aikawa K., Awaji Y., and Wada N. (2019). 1.2 Pb/s throughput transmission using a 160 μm cladding, 4-core, 3-mode fiber. IEEE J. Lightwave Technol., 37 (8), 1798-1804.

[17] Rademacher G., Puttnam B. J., Lu R. S., Klaus W., Eriksson T. A., Awaji Y., Hayashi T., Nagashima T., Nakanishi T., Taru T., Takahata T., Kobayashi T., Furukawa H., and Wada N. (2020). 10.66 peta-bit/s transmission over a 38-core-three-mode fiber. Opt. Fiber Commun. (OFC2020), Th3H. 1.

[18] Puttnam B. J., Luis R. S., Rademacher G., Galdino L., Lavery D., Eriksson T. A., Awaji Y., Furukawa H., Bayvel P., and Wada N. (2021). 0.61 Pb/s S, C, and L-band transmission in a 125 μm diameter 4-core fiber using a single wideband comb source. IEEE J. Lightwave Technol., 39 (4), 1027-1032.

[19] Rademacher G., Puttnam B. J., Lu R. S., Eriksson T. A., Fontaine N. K., Mazur M., Chen H., Ryf R., Neilson D. T., Sillard P., Achten F., Awaji Y., and Furukawa H. (2021). Peta-bit-per-second optical communications system using a standard cladding diameter 15-mode fiber. Nature Commun., 12, 4238-1-4238-7.

[20] Takenaga K., Arakawa Y., Sasaki Y., Tanigawa S., Matsuo S., Saitoh K., and Koshiba M. (2011). A large effective area multi-core fiber with an optimized cladding thickness. Opt. Express, 19 (26), B543-B550.

[21] Le Noane G., Boscher D., Grosso P., Bizeul J. C., and Botton C. (1994). Ultra high density cables using a new concept of bunched multicore monomode fibers. Proc. Int. Wire & Cable Symp., 203-210.

[22] Okamoto K. (2022). Fundamentals of Optical Waveguides. 3rd Ed. Chap. 4, Academic Press, New York.

[23] Koshiba M., Saitoh K., and Kokubun Y. (2009). Heterogeneous multi-core fibers: proposal and design principle. IEICE Electron. Express, 6 (2), 98-103.

[24] Hayashi T., Taru T., Shimakawa O., Sasaki T., and Sasaoka E. (2011). Design and fabrication of ultra-low crosstalk and low-loss multi-core fiber. Opt. Express, 19 (17), 16576-16592.

[25] Hayashi T., Taru T., Shimakawa O., Sasaki T., and Sasaoka E. (2012). Characterization of crosstalk in ultra-low-crosstalk multi-core fiber. IEEE J. Lightwave Technol., 30 (4), 583-589.

[26] Sasaki Y., Takenaga K., Guan N., Matsuo S., Saitoh K., and Koshiba M. (2012). Large-effective-area uncoupled few-mode multi-core fiber. Opt. Express, 20 (26), B77-B84.

[27] Saitoh K. and Matsuo S. (2016). Multicore fiber technology. IEEE J. Lightwave Technol., 34 (1), 55-66.

[28] Sakaguchi J., Klaus W., Delgado Mendinueta J. M., Puttnam B. J., Luis R. S., Awaji Y., Wada N., Hayashi T., Nakanishi T., Watanabe T., Kokubun Y., Takahata T., and Kobayashi T. (2016). Large spatial channel (36-core × 3 mode) heterogeneous few-mode multicore fiber. IEEE J. Lightwave Technol., 34 (1), 93-103.

[29] Hayashi T., Nagashima T., Yonezawa K., Wakayama Y., Soma D., Igarashi K., Tsuritani T., Taru T., and Sasaki T. (2017). Six-mode 19-core fiber with 114 spatial modes for weakly-coupled mode-division multiplexed transmission. IEEE J. Lightwave Technol., 35 (4), 748-754.

[30] Sekiya E. H., Saito K., Bing Y., Ogura A., and Ohsono K. (2012). Fiber fuse in multi core fibers. IEICE Technical Rep., 112 (194), 19-22.

[31] Shuto Y. (2014). Heat conduction modeling of fiber fuse in single-mode optical fibers. J. Photonics, 2014, 645207.

[32] Todoroki S. (2016). Quantitative evaluation of fiber fuse initiation with exposure to arc discharge provided by a fusion splicer. Sci. Rep., 6, 25366.

[33] Kubota M., Furuya K., and Suematsu Y. (1980). Random-bend loss-evaluation in single-mode optical fiber with various index profiles. Trans. IECE Japan, E63 (10), 723-730.

[34] Kuwaki N., Ohashi M., Tanaka C., and Uesugi N. (1985). Dispersion-shifted convex-index single-mode fibres. Electron. Lett., 21 (25), 1186-1187.

[35] Kuwaki N., Ohashi M., Tanaka C., Uesugi N., Seikai S., and Negishi Y. (1987). Characteristics of dispersion-shifted dual shape core single-mode fibers. IEEE J. Lightwave Technol., LT-5 (6), 792-797.

[36] Kawakami S. and Nishida S. (1974). Anomalous dispersion of new doubly clad optical fibre. Electron. Lett., 10 (4), 38-40.

[37] Kawakami S. and Nishida S. (1974). Characteristics of a doubly clad optical fiber with a low-index inner cladding. IEEE J. Quantum Electron., QE-10 (12), 879-887.

[38] Okamoto K., Edahiro T., Kawana A., and Miya T. (1979). Dispersion minimisation in single-mode fibres over a wide spectral range. Electron. Lett., 15 (22), 729-731.

[39] Miya T., Okamoto K., Ohmori Y., and Sasaki Y. (1981). Fabrication of low dispersion single-mode fibers over a wide spectral range. IEEE J. Quantum Electron., QE-17 (6), 858-861.

[40] Okamoto K. (2022). Fundamentals of Optical Waveguides. 3rd Ed. Chap. 5, Academic Press, New York.

[41] Agrawal G. P. (2001). Nonliear Fiber Optics. 3rd Ed. Chap. 2, Academic Press, New York.

[42] Okamoto K. (2022). Fundamentals of Optical Waveguides. 3rd Ed. Chap. 6, Academic Press, New York.

[43] Abedin K. S. and Nakazawa M. (2010). Real time monitoring of a fiber fuse using an optical time-domain reflectometer. Opt. Express, 18 (20), 21315-21321.

[44] Shuto Y. (2022). Fiber fuse simulation in dispersion-shifted fibers. J. Electrical and Electronic Eng., 10 (4), 142-148.

[45] Todoroki S. (2005). Origin of periodic void formation during fiber fuse. Opt. Express, 13 (17), 6381-6389.

[46] Kashyap R. and Blow K. J. (1988). Observation of catastrophic self-propelled self-focusing in optical fibres. Electron. Lett., 24 (1), 47-49.

[47] Atkins R. M., Simpkins P. G., and Yablon A. D. (2003). Track of a fiber fuse: a Rayleigh instability in optical waveguides. Opt. Lett., 28 (12), 974-976.